American Mineralogist, Volume 92, pages 254–260, 2007

Ionoluminescence of leucophanite

HENRIK FRIIS,[1,2,*] ADRIAN A. FINCH,[2] PETER D. TOWNSEND,[3] DAVID E. HOLE,[3] AND HASSANE EL MKAMI[4]

[1]Geological Institute, University of Copenhagen, Øster Voldgade 10, 1350 Copenhagen K, Denmark
[2]Centre for Advanced Materials and School of Geography and Geosciences, University of St. Andrews, Irvine Building, St. Andrews, Fife KY16 9AL, U.K.
[3]School of Science and Technology, University of Sussex, Pevensey Building, Falmer, Sussex BN1 9NH, U.K.
[4]School of Physics and Astronomy, University of St. Andrews, North Haugh, St. Andrews, Fife KY16 9SS, U.K.

ABSTRACT

The luminescence of three natural samples of leucophanite (ideally, $NaCaBeSi_2O_6F$) has been investigated with ion-beam excitation and by electron spin resonance (ESR). A blue luminescence, ascribed to a defect associated with SiO_4 or BeO_4 tetrahedra, and an orange luminescence, ascribed to an Mn^{2+} center, dominates the emission. Further luminescence centers in the investigated wavelength range (200–1100 nm) include those related to Gd^{3+}, Dy^{3+}, Tb^{3+}, Sm^{3+}, Eu^{3+}, Tm^{3+}, and Nd^{3+}. In spite of a sheet-like structure, leucophanite is relatively resilient to the ion implantation and β-irradiation, compared with other minerals, but loss of luminescence intensity as a function of implantation show that some permanent defects are formed. No centers change their emission energy as a function of temperature in the investigated interval (40–300 K), but due to crystal-field interaction, a broadening of the Mn^{2+} emission band is observed with increasing temperature, and with low activator concentration. The variation in activator concentration is clearly seen from a pronounced concentration quenching. ESR data (9.7 and 188 GHz) show that Mn is only present in one crystallographic site and that the REE-richest sample has an additional signal with $g \sim 2.003$. No new defects could be seen with ESR in a β-irradiated sample.

Keywords: Ionoluminescence, leucophanite, ESR, REE, Mn^{2+}, lanthanide

INTRODUCTION

The luminescence of synthetic materials has been widely investigated for applications in cathode ray tubes, laser materials, and radiation dosimetry. In addition, a smaller but significant body of literature has grown around the luminescence of geological materials, including apatite, calcite, feldspars, and zircon (see e.g., Roeder et al. 1987; Habermann et al. 1998; Götze et al. 1999; Gaft et al. 2001, 2002, 2005; Krbetschek et al. 2002). A common difference between the luminescence of synthetic and geological systems is that the number of competing luminescence centers in synthetic systems is usually constrained whereas for Earth materials, composition and states of order are extremely variable, and thus the number of potentially active luminescence centers can be very high. Understanding luminescence in minerals requires an understanding of the mechanisms controlling energy transfer between centers. In the context of minerals, this includes energy cascades within single ions, energy transfer between ions of the same species on different sites, or energy transfer between competing luminescence centers of different types. In the present study, we investigate the luminescence and electron spin resonance (ESR) of the mineral leucophanite (ideally $NaCaBeSi_2O_6F$) as a function of temperature, composition, and defect concentration to understand more about how energy deposited during excitation is dissipated to generate light. At least nine competing luminescence centers have been identified resulting in emission bands between 311 and 1060 nm. Leucophanite has a wide range of chemical exchanges from its ideal formula, notably exchange of rare earth elements (REE = lanthanides + Y) for Ca that, like defects on the SiO_4 and BeO_4 tetrahedra, give rise to light emission. The competition between these families of centers is of widespread interest since it is common to many mineral groups including apatite, feldspar, zircon, and allanite. However, leucophanite benefits from a very high luminescence efficiency, higher stability during excitation, and fewer non-equivalent crystallographic sites. It is therefore an ideal material to investigate energy transfer in a multi-doped material and provides key insights into mineral luminescence that are widely applicable to other important mineral systems.

MATERIALS AND METHODS

Leucophanite is structurally closely related to the melilite group and crystallizes in the orthorhombic space group $P2_12_12_1$. The crystal structure of the samples analyzed here was solved using single-crystal X-ray diffraction (XRD) by Friis (2004), who found no evidence for symmetry lower than orthorhombic. Therefore all Ca sites are equivalent and the coordination of an ion substituting for it is well-constrained. We chose three samples for further detailed analysis. Before selecting these samples, we examined visually the luminescence properties of a wide range of leucophanites with electron beam excitation (cathodoluminescence, CL, using a Technocyn 8200 Mk 3 Cathodoluminoscope operating to generate a power density of <100 kW/m^2) and UV excitation (photoluminescence, PL, using a MINERALIGHT Multiband Ultra-Violet Lamp type MSL-48 with both long wave and short wave).

* E-mail: geofriis@yahoo.com

0003-004X/07/0203–254$05.00/DOI: 10.2138/am.2007.2167

Natural leucophanite is divisible into blue and orange luminescent variants. The three samples chosen reflect the chemical variation observed in nature and include samples that show both orange and blue luminescence. **Leuco5** (Ref: Geological Museum of Copenhagen GM 1971.276) is greenish-yellow colored and from a pegmatite in the kakortokites (layered complex of eudialyte-, arfvedsonite-, and feldspar-rich nepheline syenites, respectively) of Kangerdluarssuk fjord, part of the Ilímaussaq alkaline complex. Semenov et al. (1987) described the pegmatite in detail. Both PL and CL are blue. **Leuco8** (Geological Museum of Copenhagen, no reference number) is from the type locality (the island of Låven in the Langesundsfjord, Norway), has a yellowish color and orange luminescence under both forms of excitation. **Leuco9** (no reference number) is the outer zone of a large irregular mass from a pegmatite from the island of Barkevikskjær in Langesundsfjord. Under UV excitation, the outer zone is blue whereas the core is orange, but in CL both zones have an orange emission. The outer zone is colorless and inclusion free contrary to the core, which contains many inclusions. This sample was kindly provided by private collector Alf Olav Larsen.

The trace-element concentrations of the samples were determined by laser ablation inductively coupled plasma mass spectrometer (LA-ICPMS) at the Natural History Museum in London. A Thermo Elemental PlasmaQuad 3 ICP-MS with S-option high efficiency interface was coupled to a New Wave Research UP-213 A1 (213 nm laser with a power density of 3.5 J/cm^2 for a 60 µm spot). NIST 612 (synthetic glass) was used as a standard for machine fluctuation correction, and CaO from EPMA was used as internal standard. The results are presented in Table 1. The compositional differences between the samples can be summarized as Leuco8 is rich in Mn, Leuco5 is rich in REE, and Leuco9 is poor in both Mn and REE.

Luminescence was generated by ion-beam implantation (ionoluminescence, IL). IL experiments have the benefit of a high power density, excitation that can be focused into a small spot (essential for minerals that are commonly heterogeneous at millimeter scales) and provide responses that are dominantly representative of the bulk. Note that other forms of excitation, notably CL, provide luminescence indicative of atypical surface states (Brooks et al. 2002). Experiments were carried out using the University of Sussex 3 MeV van de Graaf accelerator, which generated a 0.95 MeV H^+ ion beam with a current of ~50 nA and a spot size of ~0.5 cm^2. Such experimental conditions avoid neutron radiation following proton implantation into Be (a problem at higher acceleration potentials) and minimize the collision damage at the end of the ion track that can modify or degrade the sample. A fresh cleavage fragment was placed so that the incident beam hit the (001) face at an angle of ~22.5°. The light emission was collected by quartz fiber optics, placed ~45° from the incident beam, and connected to an f/4 Spectrapro 300i monochromator. A Photek image intensified CCD camera was used as a detector in the wavelength range from 200 to 1100 nm with a 2 nm resolution. Since the detector was not able to cover the entire wavelength range simultaneously, the detector was placed at different wavelengths to record spectra with 100 nm overlaps. The program WinSpec32 was used to match three spectra and generate a continuous spectrum covering the whole wavelength range. The temperature dependence was investigated in the temperature interval 40 to 300 K. An 8 W He compressor was used to reach low temperatures and Ag-dag ensured thermal contact between the compressor head and the sample. The temperature resolution in the experiment is ~10 K. All experiments were conducted with a vacuum of ~10^{-6} mbar. A linear normalization was used to correct the intensity data for variations in beam current, which was checked immediately before and after each acquisition. The intensity data were corrected for the system response using a W lamp and W emissivity data from Lide (1994).

The X-band and high field electron spin resonance (HF-ESR) experiments were conducted at the ESR Centre in the School of Physics and Astronomy at the University of St. Andrews. The high frequencies 94 and 188 GHz spectra were measured using a novel quasi-optical spectrometer that was designed and built at the University of St. Andrews. Smith et al. (1998) provided a description of the instrument. Liquid He cooling was used to acquire spectra in the temperature range ~5–300 K. The X-band experiments were conducted at room temperature on a Bruker Elexsys 580 spectrometer operating at 9.7 GHz. The samples used were crushed and hand picked before powders were prepared. Only the 188 GHz and X-band data are presented here. The sample with lowest trace-element concentration (Leuco9) was also studied before and after irradiation with a ^{90}Sr β source receiving a total dose of ~15 kGy.

TABLE 1. Trace element concentrations (in ppm) for the three leucophanite samples

n	Leuco5 6		Leuco8 7		Leuco9 5	
	Avg.	2σ	Av.	2σ	Avg.	2σ
Mn	208	35	679	84	237	50
La	1174	79	449	93	34	15
Ce	4175	245	1242	145	137	52
Pr	550	38	151	17	22	8
Nd	2467	184	576	46	91	36
Sm	480	41	121	11	19	7
Eu	41	3	11	1	2	1
Gd	354	31	108	12	14	5
Tb	40	4	17	1	2	1
Dy	198	19	102	5	10	4
Ho	29	4	18	1	2	1
Er	57	9	42	2	4	1
Tm	5	1	4	0	0	0
Yb	22	5	18	2	2	1
Lu	2	0	1	0	0	0

Note: n is number of analytical points.

RESULTS

IL spectroscopy

The light emissions from Leuco8 and Leuco5 are presented in Figures 1 and 2, respectively. A summary of the observed emissions and their proposed origins is listed in Table 2. The spectra for Leuco8 and Leuco9 are similar and dominated by a broad emission ~607 nm, which we ascribe to electronic

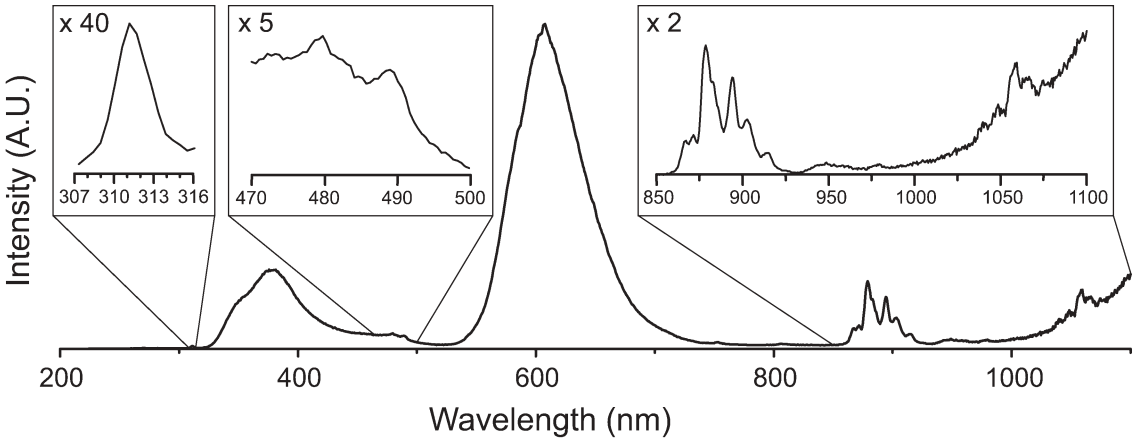

FIGURE 1. Ionoluminescence spectrum of Leuco8 at room temperature. The main emission around 600 nm is from Mn^{2+}. Insets are sections of the spectrum in greater detail to show the Gd^{3+}, Dy^{3+}, and Nd^{3+} emissions, respectively.

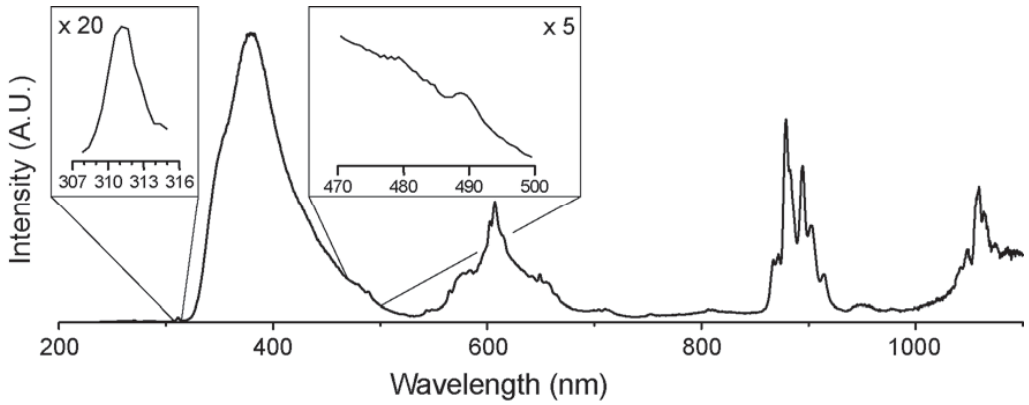

FIGURE 2. Ionoluminescence spectrum of Leuco5 at room temperature. No Mn^{2+} emission is observed but rather a series of line emissions from primarily Sm^{3+}. The spectrum is dominated by an emission around 380 nm (see text for discussion of this center). Insets are sections of the spectrum in greater detail to show the Gd^{3+} and Dy^{3+} emissions, respectively.

TABLE 2. Major luminescence centers observed in leucophanites with possible origins and suggested electronic transitions

Wavelength (nm)	Activator	Photon energy (eV)	Possible electronic transitions
311	Gd^{3+}	3.99	$^6P_{7/2} \rightarrow {}^8S_{7/2}$
380	O^-	3.26	
479	Dy^{3+}	2.59	$^4F_{9/2} \rightarrow {}^6H_{15/2}$
489	Dy^{3+}	2.54	
543	Tb^{3+}	2.28	$^5D_4 \rightarrow {}^7F_5$
565	Sm^{3+}	2.19	$^4G_{5/2} \rightarrow {}^6H_{5/2}$
578*	Dy^{3+}	2.14	$^4F_{9/2} \rightarrow {}^6H_{13/2}$
584*	Tb^{3+}	2.12	$^5D_4 \rightarrow {}^7F_4$
602	Sm^{3+}	2.06	$^4G_{5/2} \rightarrow {}^6H_{7/2}$
607	Mn^{2+}	2.04	$^4T_1 \rightarrow {}^6A_1$
607	Sm^{3+}	2.04	$^4G_{5/2} \rightarrow {}^6H_{7/2}$
615	Eu^{3+}	2.01	$^5D_0 \rightarrow {}^7F_2$
642	Sm^{3+}	1.93	$^4G_{5/2} \rightarrow {}^6H_{9/2}$
649	Sm^{3+}	1.91	
655	Sm^{3+}	1.89	
665	Dy^{3+}	1.86	$^4F_{9/2} \rightarrow {}^6H_{11/2}$
807	Tm^{3+}	1.54	$^3F_4 \rightarrow {}^3H_6$
879	Nd^{3+}	1.41	$^4F_{3/2} \rightarrow {}^4I_{9/2}$
894	Nd^{3+}	1.39	
1060	Nd^{3+}	1.17	$^4F_{3/2} \rightarrow {}^4I_{11/2}$

* Both emissions could originate from either Dy or Tb or both.

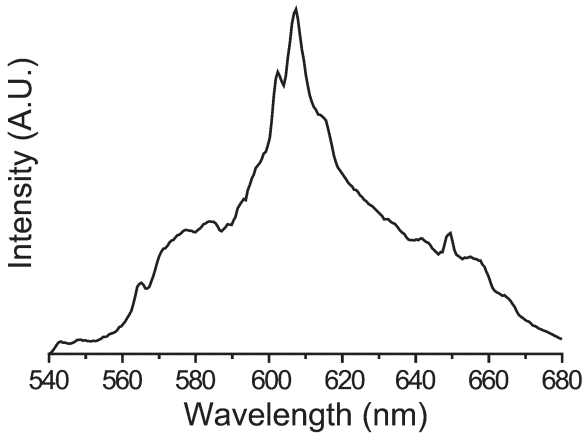

FIGURE 3. Detailed section of Leuco5 showing the complex emissions in the region around 600 nm. See Table 2 for assignment of activators to individual emissions. The intensity axis is magnified 2.5× compared to Figure 2.

transitions within Mn^{2+} as described for natural and synthetic leucophanite (Gorobets and Prokofiev 1981; Prokofiev et al. 1982). A series of emissions around 900 nm, a single peak at 311 and a doublet at 480 and 490 nm are present in all the samples and we attribute these to electronic transitions in Nd^{3+}, Gd^{3+}, and Dy^{3+}, respectively, by analogy with earlier published data (Gorobets and Prokofiev 1981; Prokofiev et al. 1982; Gorobets and Rogojine 2002; Gaft et al. 2005). However, the Gd^{3+} emission has not been reported before in leucophanite but is found in other mineral systems, e.g., REE-bearing zircon (Karali et al. 2000). A broad band in the blue-UV around 380 nm is present in all three samples. The spectra of Leuco5 (Fig. 2) have many features in common with the other two, but the broad emission at ~382 nm dominates. In Leuco5, the yellow-orange band around 600 nm has a series of sharp peaks and this feature most probably results from the superposition of emissions related to electronic transitions in predominantly Sm^{3+} with minor contributions from Eu^{3+}, Tb^{3+}, Dy^{3+}, and Mn^{2+} (see Fig. 3 for a detail spectrum of the region). The spectra in the present study correspond well to published PL, X-ray luminescence and laser-induced spectra of natural and synthetic leucophanite (Gorobets and Prokofiev 1981; Prokofiev et al. 1982; Gorobets and Rogojine 2002; Gaft et al. 2005).

Ion implantation modifies the luminescence efficiency and almost always causes intensity decreases. After implantation of $\sim 2 \times 10^{14}$ H^+ ions, the luminescence intensity decreased by ~10%, significantly less than that reported for feldspars (Brooks et al. 2002; Finch et al. 2003), zircon (Finch et al. 2004), and other minerals including sodalite, charoite, and fluorite (Finch et al. unpublished data). After 12 hours without irradiation, no recovery in the intensity of the emissions was observed. All emission bands showed a decrease in intensity with increasing temperature (Table 3). Two new emissions were observed as the temperature increased: a singlet at ~807 and a doublet at ~870 nm. The full-width at half-maximum (FWHM) of the Mn emission increased ~150 and ~100 K for Leuco8 and Leuco9, respectively, which is the temperature range where Suyver et al. (2003) also observed broadening of FWHM for the Mn^{2+} emission in nanocrystals of ZnS doped with Mn. The total change in FWHM is 6 and 16 nm for Leuco8 and Leuco9, respectively.

ESR

The HF-ESR (188 GHz) of all three samples (Fig. 4) is dominated by the sextet, known as hyperfine structure, originating from the interaction between the unpaired electrons and ^{55}Mn nucleus with $I = 5/2$ (100% natural abundance) and correlates with the presence of the broad Mn^{2+} luminescence band. As the Mn has more than one unpaired electron ($S = 5/2$), the interaction between spins, called zero-field splitting (ZFS), leads to a removal of degeneracy of spin levels even without any external magnetic field. The ESR spectrum is then characterized by the axial (D) and rhombic (E) ZFS parameters that provide a measure of the deviation from the ideal octahedral and tetrahedral symmetries, which cause the sextet to be split into 18 lines because the *g*-value is orientation dependent in the low symmetry coordination. From the inset in Figure 4, it can be seen that each line in the sextet is split into three (only obvious at the high-field end of the spectra). When the energy of ZFS is larger than Zeeman energy, the allowed ESR transitions spread out over a broad magnetic field range and cannot always be observed with low frequencies (Fig. 5). Therefore, the use of high frequencies becomes necessary to overcome these kinds of problems. The three signals in the inset of Figure 4 have been plotted using the same scale so the relative intensities among the samples are directly comparable. The signal is almost equal for Leuco5 and Leuco9, but much stronger for Leuco8, which corresponds with the relative Mn concentrations in the samples (Table 1). The 188 GHz spectrum for Leuco5 provides better *g*-value resolution and shows an additional peak at the end of the Mn^{2+} sextet that can be related to another species with $g \sim 2.003$. The same feature can be seen more clearly at X-band because the ZFS effect spreads out the Mn contribution (see the inset in Fig. 5) and the extra feature appears more intense. The X-band and high-field results suggest that the manganese ion is present in a low symmetry site and this assumption is well supported by the *g* anisotropy shown at high field and the large zero-field splitting parameters observed at X-band. The only temperature dependence observed was an increase in amplitude with decreasing temperature for Leuco5 and Leuco9 with low Mn^{2+} concentration, whereas the opposite is the case for Leuco8. The behavior of Leuco8 can be related to the larger Mn^{2+} concentration that leads to dipole-dipole interactions and therefore induces a broadening of the ESR lines or to a relaxation phenomenon.

The irradiated sample was only run at high field and compared to the unirradiated sample by scaling and subtracting the two spectra. No significant residual was found that would indicate the presence of a radiation-generated defect.

TABLE 3. Relative intensity decrease for the major emission centers as $I_{(300\ K)}/I_{(37\ K)}$

Center	O^-	Mn^{2+}	Sm^{3+}	Nd^{3+}
λ	380	607	607	879
Leuco5	0.57		0.41	0.57
Leuco8	0.61	0.51		0.64
Leuco9	0.58	0.84		0.94

Note: λ is the wavelength in nm.

DISCUSSION

Stability

The program SRIM2003 (Ziegler and Biersack 2003) was used to conduct Monte-Carlo simulations of the effect of irradiation with 0.95 MeV H^+ ions on leucophanite (10^5 ions). With a density of 2.95 g/cm^3, simulations suggest that the protons penetrated to a depth of 11.2 µm. More than 99.8% of the energy is deposited via electronic excitation of the lattice and this can decay via a mixture of luminescence or lattice vibrations. The remaining 0.2% of the energy primarily forms lattice displacements near the end of the ion track. Lattice defects may also be caused by the ionization effect during ion-beam implantation but the efficiency is very variable among materials ranging from high in halides, to low (but finite) in silica, to negligible in many oxides (Townsend et al. 1994). Leucophanite, $NaCaBeSi_2O_6F$, will therefore probably form some defects throughout the ion range as a result of the ionization energy transfer. In ion bombardment terms, 2×10^{14} H^+ ions/cm^2 is a relatively modest defect-forming dose. It will, however, result in charge transfers between existing defect sites as well as stimulating transient defect signals. The

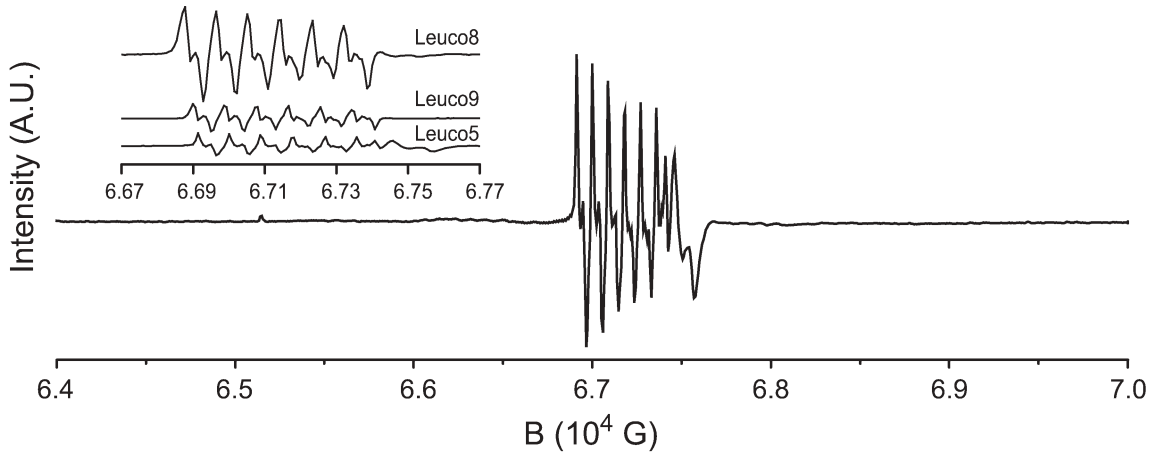

FIGURE 4. 188 GHz ESR spectrum of Leuco5 at room temperature showing the hyperfine structure of Mn^{2+}, with an extra feature present in the end of the spectrum. Due to low site symmetry of Mn, *g* is split into three individual lines. The inset shows in detail the splitting of *g* causing the decomposition of each line into three. The amplitudes are normalized, so a direct comparison of the signal intensity among the three samples is possible.

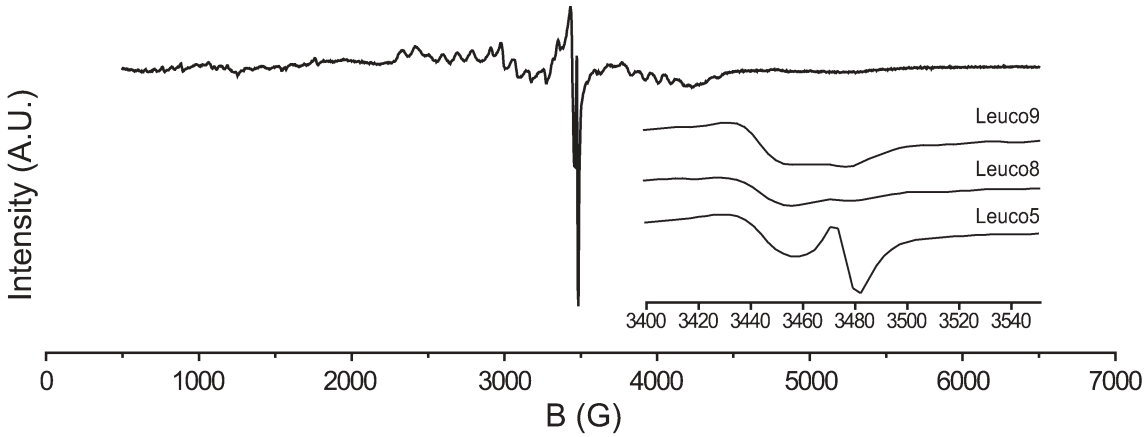

FIGURE 5. X-band spectrum of Leuco5 at room temperature showing the zero-field splitting and the feature with $g \sim 2.003$. The inset shows in detail the region with the extra center present in Leuco5 that is not found in the other samples.

observed ~10% decrease in signal intensity therefore suggests that changes must exist throughout the ion range, and not merely in the last few percent where there is nuclear collision damage. The data thus imply that ionization-derived defect formation occurs in this material. The defects are believed to be permanent or long-term metastable defects, since no recovery of the intensity was observed when the samples were left for 12 hours. The fact that the intensity decrease during irradiation is relatively small indicates that leucophanite is resilient to much of the ion damage. The conditions were chosen to result in minimal vacancies and displaced atoms (<0.01%). Nevertheless, light ions such as Be, O, and Al in sheet-like structures, might have relatively low displacement energies and therefore a single implanted ion may cause atomic displacements. However, our observations suggest there is only a small, albeit measurable, damage effect at the dose levels required for ion-beam luminescence characterization. It may be, for example, that displaced atoms quickly recover to their original positions. This recovery is also supported by the HF-ESR data for the β-irradiated sample that did not show any modification of the Mn^{2+} ESR response or the presence of new defects related to displaced atoms.

Temperature

Table 3 presents the intensity of major emissions as a function of temperature. Our temperature experiments revealed no evidence of a phase transition of leucophanite, which is supported by comparisons of single-crystal XRD at 120 K and room temperature (Friis 2004), and by our temperature-dependent HF-ESR data. Luminescence intensity does, however, decrease with increasing temperature and the degree of quenching varies among the samples. The emissions from Gd^{3+} and Dy^{3+} are not included because their intensities are small and overlap with more intense and broader emission bands. Studies of the thermal behavior of luminescence gives insights into the manner in which thermal charge transfer contributes to dissipating energy between competing luminescence centers. All of the spectra show lower luminescence intensities at room temperature compared to 40 K, demonstrating that more of the energy deposited is dissipated by thermal vibrations. The broadening of the luminescence emissions demonstrates the role of lattice vibrations in the recombination process. For example, the yellow luminescence from Mn^{2+} is believed to arise from a partly spin-forbidden transition and is therefore coupled with quantized lattice vibration (phonon) (e.g., Telfer and Walker 1978). The increase of the FWHM of the Mn^{2+} emission (i.e., less increase with increased concentration) is consistent with a model whereby the luminescence centers behave as a variety of isolated or partly interacting centers in Leuco9. Leuco8 has a higher concentration of Mn giving rise to strong coupling between centers, and hence a more uniform luminescence behavior. Suyver et al. (2003) showed that in nanocrystalline ZnS:Mn^{2+}, the $^4T_1 \rightarrow {}^6A_1$ transition of Mn^{2+} is strongly coupled with the crystal field, which decreases with increasing temperature resulting in a shift of peak position toward higher emission energy. Such a shift has not been observed for the Mn^{2+} emission in leucophanite. The difference in thermal quenching among the samples is coupled with the concentration of the activator in the sample and reflects the degree of self-quenching.

The 807 nm emission occurring at high temperatures could be a low energy transition corresponding to the $^3F_4 \rightarrow {}^3H_6$ transition in Tm^{3+} (Blanc et al. 2000). Another possibility is the $^3P_1 \rightarrow {}^1G_4$ in Pr^{3+}, which is only observed close to room temperature in zircons (Finch et al. 2004). However, two emissions at ~870 nm are only observed at high temperature, and these has been related to Tm^{3+} by Gaft et al. (2005). Hence, we find it likely that all three emissions are related to Tm^{3+}, rather than to Nd^{3+}. A low-temperature emission at ~580 (Leuco5) is believed to be a low-energy transition within Tb^{3+} or Dy^{3+}.

Luminescence centers in leucophanite

The leucophanites show sharp peaks in the blue-UV region at 311 nm that are attributed to transitions within the Gd^{3+} ion (Table 2). However, the most obvious feature in the spectra of all the samples in this region is a broad blue-UV band centered around 380 nm. The origins of broad blue-UV emissions in minerals are often the subject of debate. It can be seen in Table 3 that the thermal quenching of the 380 nm emission is ~60% in all samples despite the wide variations in trace element contents. This is inconsistent with emission from a particular ion such as a lanthanide (Ce^{3+}), as suggested by Gorobets and Prokofiev (1981)

and Prokofiev et al. (1982). The former authors suggested that the emission might be related to a defect e.g., O^- or F^-. Broad emission bands around 380 nm have, in many minerals, been ascribed to electron-hole recombination associated with centers on tetrahedral sites, e.g., $[AlO_4]^0$ center in quartz (Martini et al. 1995) or [Si-O-Si, Si-O-Al, or Al-O-Al] as described in feldspars (Finch and Klein 1999; Garcia-Guinea et al. 1999). If we accept that the broad blue-UV emission is a defect-related phenomenon, then it might be the result of the ion implantation that is used to excite the sample. Ion implantation can modify samples in real time, generating luminescence centers that did not previously exist. However, Gorobets and Prokofiev (1981), Prokofiev et al. (1982), and our unpublished data show the blue emission is also present when excited by lower energy methods (PL). Since the energy deposited by PL is a few eV, such excitation is insufficient to create new defects, and the luminescence intensity does not increase during progressive implantation.

Another possibility is that the emission is caused by an exciton formed during an electron-hole relaxation, which gives energies around 3 eV (~400 nm). Variations in locality from different hosts or defect sites modify the dielectric constants so the energy shifts slightly. Korotaev et al. (2002) investigated emissions around 380 nm in three Be-minerals (beryl, chrysoberyl, and phenakite) and found them to be related to centers with ns lifetimes. They ascribed the centers to intrinsic luminescence and found them to vary slightly in emission energy depending on excitation energy and crystal structure. Similar discussion exists for many other insulators, for example the wavelength shifts of the decay of excited exciton states in silica quartz, and other silicates have been ascribed to impurity perturbations of decay sites (e.g., Yang and McKeever 1990; Stevens and Phillips 1995; Stevens 1998). Therefore, we attribute the 380 nm emission at least in part to an intrinsic process, perhaps electron-hole recombination near an SiO_4 or BeO_4 tetrahedron. Further work studying luminescence lifetimes is underway to explore this possibility.

Sample Leuco5, which has the most intense blue-UV luminescence, shows evidence for an extra paramagnetic center in ESR, which is absent in the other two samples. This sample has the highest REE content, and Friis (2004) showed that the incorporation of REE generates a Ca vacancy. The extra ESR feature has a superficial resemblance to descriptions of ESR responses of Ca vacancies in other structures (e.g., Onori et al. 1998; Bortolin and Onori 2005). Such a vacancy might be capable of capturing an electron hole, and therefore relate to the 380 nm emission. However, it is considered most likely that this feature is related to an REE ion and this will be the subject of a future ESR publication, which will include modeling the response at several frequency bands.

IMPLICATIONS

Our studies provide important insights into the luminescence of the leucophanite system that in turn affords analogies with other minerals in which several luminescence centers compete. Luminescence intensities in leucophanite, as in other systems (e.g., zircon, Finch et al. 2004), do not correlate with REE content, which shows that recombination pathways involving some particular REEs are preferred to others. Hence, luminescence from Tm^{3+} is observed even though this element is among the least abundant in the material (Table 1). Furthermore, both Gd^{3+} and Dy^{3+} are observed in all samples although their concentrations vary significantly among the samples. The energy of the conduction band in leucophanite may coincide with permitted energy levels in these REE ions thus facilitating energy transfer from the conduction band. Alternatively, other centers, e.g., other lanthanides, may mediate the energy transfer. Thermally assisted promotion of electrons to higher energy levels becomes more important at higher temperatures, creating new recombination pathways via which energy may return to the ground state. In addition, temperature causes the width and mean energies of bands associated with each lanthanide to change, opening and closing energy pathways as energy bands in adjacent ions overlap. Energy transfer involving coupling with phonons is also important (e.g., Mn).

Leucophanite is an excellent material in which to study competition between alternative luminescence centers. Its high quantum efficiency, stability in the ion beam, and the restricted coordination available to lanthanides mean that it is a relatively simple mineral to understand. The types of competing recombination pathways observed in leucophanite are undoubtedly present in several common mineral systems such as apatite, zircon, and allanite, which share the combinations of REE, Mn, and defect-related luminescence centers.

By not being as surface-dependent as, e.g., CL, ionoluminescence proved efficient in stimulating energy transfer between several competing elements in leucophanite. The intensity of the different emission bands, as a function of ion dose, can be used as a proxy for the response of the material to implantation-created defects and hence provide knowledge of the materials suitability as, e.g., storage for nuclear waste. With changing temperature, IL responses from different activators enabled us to distinguish between elements and intrinsic defects, something that is often compromised by the huge surface effect of CL.

ACKNOWLEDGMENTS

This study was supported by a NERC standard grant. H.F. gratefully acknowledges receipt of bursaries from the University of St. Andrews and the Natural History Museum in London and A.A.F. acknowledges tenureship of a BP/Royal Society of Edinburgh fellowship. Private collector Alf Olav Larsen and the Geological Museum in Copenhagen are thanked for supplying samples for this study. The ESR centre in St. Andrews is funded by EPSRC and the authors thank G. Smith for helpful discussions. Raquel Garcia-Sanchez (Natural History Museum, London, U.K.) collected the LA-ICPMS data. Joel Spencer (University of Innsbruck, Austria) assisted with the β irradiation. We thank reviewers M. Gaft and N.R.J. Poolton for their constructive comments that increased the quality of the paper. We also thank Associate Editor P. Edwards for handling the manuscript.

REFERENCES CITED

Blanc, P., Baumer, A., Cesbron, F., Ohnenstetter, D., Panczer, G., and Remond, G. (2000) Systematic cathodoluminescence spectral analysis of synthetic doped minerals: anhydrite, apatite, calcite, fluorite, scheelite, and zircon. In M. Pagel, V. Barbin, P. Blanc, and D. Ohnenstetter, Eds., Cathodoluminescence in Geosciences, p. 127–160. Springer, Berlin.

Bortolin, E. and Onori, S. (2005) Features of EPR dosimetry with $CaSO_4$:Dy phosphor. Applied Radiation and Isotopes, 62, 349–352.

Brooks, R.J., Finch, A.A., Hole, D.E., Townsend, P.D., and Wu, Z. (2002) The red to near-infrared luminescence in alkali feldspar. Contribution to Mineralogy and Petrology, 143, 484–494.

Finch, A.A. and Klein, J. (1999) The causes and petrological significance of cathodoluminescence emissions from alkali feldspars. Contribution to Mineralogy and Petrology, 135, 234–243.

Finch, A.A., Hole, D.E., and Townsend, P.D. (2003) Orientation dependence of luminescence in plagioclase. Physics and Chemistry of Minerals, 30, 373–381.

Finch, A.A., Garcia-Guinea, J., Hole, D.E., and Townsend, P.D. (2004) Ionolu-

minescence of zircon: rare earth emissions and radiation damage. Journal of Physics D: Applied Physics, 37, 2795–2803.
Friis, H. (2004) A Study of Paragenesis, Crystal Structure and Luminescence Properties of Leucophanite, 100 p. M.Sc. thesis, University of Copenhagen, Denmark.
Gaft, M., Panczer, G., Reisfeld, R., and Uspensky, E. (2001) Laser-induced time-resolved luminescence as a tool for rare-earth elements identification in minerals. Physics and Chemistry of Minerals, 28, 347–363.
Gaft, M., Seigel, H., and Panczer, G.R. (2002) Laser-induced time-resolved luminescence spectroscopy of Pb^{2+} in minerals. European Journal of Mineralogy, 14, 1041–1048.
Gaft, M., Reisfeld, R., and Panczer, G. (2005) Luminescence Spectroscopy of Minerals and Materials, 356 p. Springer, Berlin.
Garcia-Guinea, J., Townsend, P.D., Sanchez-Muñoz, L., and Rojo, J.M. (1999) Ultraviolet-blue ionic luminescence of alkali feldspars from bulk and interfaces. Physics and Chemistry of Minerals, 26, 658–667.
Gorobets, B.S. and Prokofiev, I.V. (1981) Luminescence of beryllium minerals. Izvestiya Akademii Nauk SSSR Seriya Geologicheskaya, 4, 117–130 (in Russian).
Gorobets, B.S. and Rogojine, A.A. (2002) Luminescent Spectra of Minerals. 300 p. RPC VIMS, Moscow.
Götze, J., Habermann, D., Neuser, R.D., and Richter, D.K. (1999) High-resolution spectrometric analysis of rare earth elements-activated cathodoluminescence in feldspar minerals. Chemical Geology, 153, 81–91.
Habermann, D., Neuser, R.D., and Richter, D.K. (1998) Low limit of Mn^{2+}-activated cathodoluminescence of calcite: state of the art. Sedimentary Geology, 116, 13–24.
Karali, T., Can, N., Townsend, P.D., Rowlands, A.P., and Hanchar, J.M. (2000) Radioluminescence and thermoluminescence of rare earth element and phosphorus-doped zircon. American Mineralogist, 85, 668–681.
Korotaev, A.V., Ivanyuk, V.Y., Pustovarov, V.A., Kruzhalov, A.V., and Shulgin, B.V. (2002) Time-resolved spectroscopy of complex scintillators Al_2BeO_4, Be_2SiO_4, and $Al_2Be_3Si_6O_{18}$. Nuclear Instruments and Methods in Physics Research A, 486, 417–421.
Krbetschek, M.R., Götze, J., Irmer, G., Rieser, U., and Trautmann, T. (2002) The red luminescence emission of feldspar and its wavelength dependence on K, Na, Ca—composition. Mineralogy and Petrology, 76, 167–177.
Lide, D.R. (1994) CRC Handbook of Chemistry and Physics, p. 2380. CRC Press, Inc., Boca Raton, Florida.
Martini, M., Paleari, A., Spinolo, G., and Vedda, A. (1995) Role of $[AlO_4]^0$ centers in the 380-nm thermoluminescence of quartz. Physical Review B, 52, 138–142.
Onori, S., Bortolin, E., Lavalle, M., and Fuochi, P.G. (1998) $CaSO_4$:Dy phosphor as a suitable material for EPR high dose assessment. Radiation Physics and Chemistry, 52, 549–553.
Prokofiev, I.V., Gorobets, B.S., Gaft, M.Z., and Lurie, Y.S. (1982) Rare earth centers of luminescence in leucophanite, shortite, meionite, and monazite. Mineralogicheskij sbornik Lvovskogo universiteta, 36, 76–79 (in Russian).
Roeder, P.L., Mac Arthur, D., Ma, X.P., Palmer, G.L., and Mariano, A.N. (1987) Cathodoluminescence and microprobe study of rare-earth elements in apatite. American Mineralogist, 72, 801–811.
Semenov, E.I., Bohse, H., Sørensen, H., and Kataeva, S.T. (1987) Leucophanite in alkaline pegmatites from Ilímaussaq. Mineralogicheskii Zhurnal, 9(2), 84–85 (in Russian).
Smith, G.M., Lesurf, J.C.G., Mitchell, R.H., and Riedi, P.C. (1998) Quasi-optical cw mm-wave electron spin resonance spectrometer. Reviews of Scientific Instruments, 69(11), 3924–3937.
Stevens Kalceff, M.A. (1998) Cathodoluminescence microcharacterization of the defect structure of irradiated hydrated and anhydrous fused silicon dioxide. Physical Review B, 57, 5674–5683.
Stevens Kalceff, M.A. and Phillips, M.R. (1995) Cathodoluminescence microcharacterization of the defect structure of quartz. Physical Review B, 52, 3122–3134.
Suyver, J.F., Kelly, J.J., and Meijerink, A. (2003) Temperature-induced line broadening, line narrowing and line shift in the luminescence of nanocrystalline ZnS:Mn^{2+}. Journal of Luminescence, 104, 187–196.
Telfer, D.J. and Walker, G. (1978) Ligand field bands of Mn^{2+} and Fe^{3+} luminescence centres and their site occupancy in plagioclase feldspars. Modern Geology, 6, 199–210.
Townsend, P.D., Chandler, P.J., and Zhang, L. (1994) Optical effects of ion implantation. 294 p. Cambridge University Press, U.K.
Yang, X.H. and McKeever, S.W.S. (1990) Pre-dose effect in crystalline quartz. Journal of Physics D: Applied Physics, 23, 237–244.
Ziegler, J.F. and Biersack, J.P. (2003) SRIM-2003-20. Freeware, Annapolis, Maryland (www.srim.org).

MANUSCRIPT RECEIVED NOVEMBER 23, 2005
MANUSCRIPT ACCEPTED SEPTEMBER 21, 2006
MANUSCRIPT HANDLED BY PAUL EDWARDS